The Astrophysical Journal, 893:126 (9pp), 2020 April 20 https://doi.org/10.3847/1538-4357/ab8222

Astrophysical $S(E)$ for the ^{9}Be(p, d)^{8}Be and ^{9}Be(p, α)^{6}Li Reactions by Direct Measurement

Qian Zhang[1], Zhenglin Huang[1], Jun Hu[2,3,4], Bingjun Chen[1], Suqing Hou[2], Tieshan Wang[1], and Kaihong Fang[1,4]
[1] School of Nuclear Science and Technology, Lanzhou University, Lanzhou, Gansu Province 730000, People's Republic of China; fangkh@lzu.edu.cn
[2] Institute of Modern Physics, Chinese Academy of Sciences, Lanzhou 730000, People's Republic of China; hujunbaggio@impcas.ac.cn
[3] School of Nuclear Science and Technology, University of Chinese Academy of Sciences, Beijing 100049, People's Republic of China
Received 2019 September 7; revised 2020 February 29; accepted 2020 March 20; published 2020 April 23

Abstract

The p–^{9}Be reactions play a key role in accurate prediction of the primordial abundance of beryllium, and its abundance can be used to exquisitely probe the nucleosynthesis and mixing mechanism of stars. In the present work, astrophysical $S(E)$ factors of the ^{9}Be(p, d)^{8}Be and ^{9}Be(p, α)^{6}Li reactions have been obtained from the thick-target yield $Yield(E_i)$ for proton energies from 18 to 100 keV. A full R-matrix analysis was performed to fit both the ^{9}Be(p, α)^{6}Li and ^{9}Be(p, d)^{8}Be reactions simultaneously. The resulting astrophysical $S(E)$ factors agree well with direct measurements, leading to $S(0) = 17.3 \pm 2.1$ and 13.9 ± 1.8 MeV·b for the ^{9}Be(p, α)^{6}Li and ^{9}Be(p, d)^{8}Be reactions, respectively. However, the obtained screening potential ($U_s = 512 \pm 77$ eV) is lower than results of previous work (900 ± 50 and 806 eV), and all of them are larger than the adiabatic limit of 264 eV. The reaction rates were also calculated in the temperature range $(0.01–1) \times 10^9$ K, which improves on the precision of the standard database NACRE and NACRE II.

Unified Astronomy Thesaurus concepts: Nuclear reaction cross sections (2087); Reaction rates (2081); Nucleosynthesis (1131)

1. Introduction

The abundance of the light elements Li, Be, B (LiBeB) is one of the most interesting problems in astrophysics, along with primordial big bang nucleosynthesis (BBN) and stellar evolution (Fowler 1984; Boyd & Kajino 1989). Abundance measurements of LiBeB can provide a powerful test to differentiate between inhomogeneous and homogeneous theoretical models, and to understand the consumption mechanism in stars (Boyd & Kajino 1989; Kajino & Boyd 1990; Boesgaard & King 1993). For instance, as Brune et al. (1998) stated, the standard big bang model (homogeneous, Copi et al. 1995; Coc et al. 2012) predicts very low ^{9}Be production [$n(^9\mathrm{Be})/n(\mathrm{H}) \sim 10^{-19}$], while the non-standard big bang model (inhomogeneous, Boyd & Kajino 1989; Thomas et al. 1994) predicts significantly greater ^{9}Be production, which may be at a level observable with present technology, $n(^9\mathrm{Be})/n(\mathrm{H}) \sim 10^{-13}$.

For stars having convection zones deep enough to reach inner layers, the temperature at the base of the convection zone is high enough to ensure that Be can be easily ignited. Zero-age main-sequence stars of subsolar mass display abundances that reveal the history of the bottom of their convective zone (Brown 1998). Unfortunately, the beryllium abundance is very difficult to observe because its resonance lines are located in the near-UV spectral region of cool stars (Stephens et al. 1997).

In both stellar and primordial environments, LiBeB is mainly depleted by proton capture (e.g., in stellar models ^{9}Be is destroyed by the ^{9}Be(p, α)^{6}Li and ^{9}Be(p, d)^{8}Be reactions) within a Gamow energy (E_G) ranging from 10 keV (for stellar nucleosynthesis) to 100 keV (for primordial nucleosynthesis), which makes it an exquisite probe of depletion mechanisms in stellar evolution and inhomogeneous BBN (Boesgaard & King 1993; Rauscher et al. 1994; Primas et al. 1997; Brown 1998; Romano et al. 2006; Lamia et al. 2015). The ratio between the ^{9}Be(p, α)^{6}Li and ^{9}Be(p, 2α)^{2}H reaction rates in stellar conditions at the temperature of interest is ~1.2 (Lamia et al. 2015), and also the ^{9}Be(p, 2α)^{2}H reaction is one of the key reactions inhibiting the creation of heavier elements in the BBN model with non-uniform baryon density (Rauscher et al. 1994). However, reaction rates for the Be destruction channels ^{9}Be(p, α)^{6}Li and ^{9}Be(p, d)^{8}Be still have large uncertainties owing to large errors induced by extrapolation to the low energy of astrophysical interest, e.g., reaction rates compiled by NACRE and NACRE II (Angulo et al. 1999; Xu et al. 2013). Thus, in order to accurately calculate the depletion of ^{9}Be, the rates for these reactions must be known at stellar energies.

Additionally, Be is also considered as a candidate plasma-facing material for a fusion reactor for the utilization of nuclear energy (Federici et al. 2001; Causey 2002; Wu 2007). In the above fields, beryllium will be exposed to a keV irradiation field, and its nuclear reaction cross section in that energy region is very important and should be measured accurately. Thus, experimental research about Be is of great importance for nuclear astrophysics and the design of fusion reactors.

In general, it is advantageous to transform $\sigma(E)$ into the astrophysical $S(E)$ factor, which varies more smoothly with decreasing energy E, and is defined by (Rolfs & Rodney 1988)

$$\sigma(E) = \frac{S(E)}{E} \exp[-2\pi\eta(E)], \quad (1)$$

where E is the incident energy in the center-of-mass (c.m.) system, and $\eta(E) = Z_1 Z_2 \alpha(\mu c^2/2E)^{1/2}$ is the corresponding Sommerfeld parameter (Z_1 and Z_2 are atomic numbers of the target and projectile, α the fine structure constant, μ the reduced mass in amu, and c the velocity of light). $S(E)$ is the astrophysical factor of bare nuclei and includes all nuclear effects (Rolfs & Rodney 1988).

In the laboratory environment, target and projectile are usually both in the form of neutral atoms, molecules, or ions.

[4] Corresponding authors.

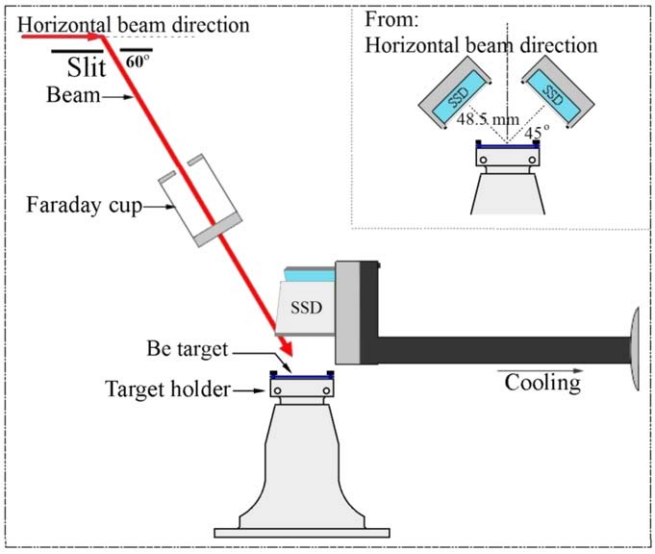

Figure 1. Schematic diagram of the setup in the experimental chamber.

Thus, the charged-particle-induced cross section is enhanced (usually) by environmental charges surrounding the interacting nuclides, with an enhancement factor (Assenbaum et al. 1987)

$$f(E) = \frac{E}{E + U_s} \exp\left(\pi\eta \frac{U_s}{E}\right), \quad (2)$$

where U_s is the screening potential provided by the environmental charges (bound/free electrons, ions) (Kittel 1986; Kasagi 2004; Raiola et al. 2004; Fang et al. 2011, 2015a, 2015b, 2016; Wang et al. 2012), which is estimated to be a constant leading to an increase in the incident energy, i.e., $E' = E + U_s$. The screening potential can be estimated via the adiabatic limit due to the bound electrons (Bracci et al. 1990). For astrophysical environments, the interacting nucleus is placed in a plasma condition; the cross section should be modified by a factor that depends on plasma properties, i.e., the Debye–Huckel theory (Salpeter 1954; Pizzone et al. 2004; Ichimaru 2008).

So far, four direct measurements of the ^{9}Be(p, α)^{6}Li and ^{9}Be(p, d)^{8}Be reactions have been reported at low energy ($E < 100$ keV) (Sierk & Tombrello 1973; Zahnow et al. 1997; Brune et al. 1998; Fang et al. 2018). Sierk & Tombrello (1973) have measured both the ^{9}Be(p, α)^{6}Li and ^{9}Be(p, d)^{8}Be reactions from 30 to 700 keV, giving the sum of $S(0) = 35^{+45}_{-15}$ MeV·b. From their results, the same $S(0) = 17^{+25}_{-7}$ MeV·b is extrapolated for both the ^{9}Be(p, α)^{6}Li and ^{9}Be(p, d)^{8}Be reactions (Angulo et al. 1999). Zahnow et al. (1997) studied the ^{9}Be(p, α)^{6}Li and ^{9}Be(p, d)^{8}Be reactions down to 16 keV, giving $S(0) = 16.1$ and 14.5 MeV·b, respectively, and $U_s = 900 \pm 50$ eV. Brune et al. (1998) studied both the ^{9}Be(p, α)^{6}Li and ^{9}Be(p, d)^{8}Be reactions with incident energies 77 keV $\leqslant E \leqslant$ 321 keV, and analyzed the data using R-matrix and direct reaction calculations, while they did not explicitly give the cross section. Recently, our group reported the $S(E)$ factor for the ^{9}Be(p, α)^{6}Li reaction from 18 to 100 keV (Fang et al. 2018), found that the ^{9}Be(p, α)^{6}Li reaction can be interpreted by one broad resonance ($J^\pi = 1^-$) including interference effects with a direct process, and agreed with R-matrix analysis. We extracted $S(0) = 16.1 \pm 1.8$ MeV·b and $U_s = 545 \pm 98$ eV.

To overcome the Coulomb barrier and avoid the effect of the screening potential, the Trojan-Horse Method (THM; Baur 1986; Spitaleri et al. 2011) has been developed and widely used. The ^{9}Be(p, α)^{6}Li reaction has been studied by Romano et al. (2006) and Wen et al. (2008) using the quasi-free condition of the ^{2}H(^{9}Be, ^{6}Liα)n reaction. For instance, Wen et al. (2008) gave $S(0) = 21.0 \pm 0.8$ MeV·b and $U_s = 676 \pm 86$ eV. However, the THM data are higher than direct data at low energies $E < 260$ keV; e.g., the result of Wen et al. (2008) is about 28% larger than that obtained from Zahnow et al. (1997) at $E_{c.m.} = 140$ keV; Romano et al. (2006) reported only two energy points below the resonance region with poor resolution. Barker & Kondō (2001) used the R-matrix method to reanalyze the experimental data (Sierk & Tombrello 1973; Zahnow et al. 1997; Brune et al. 1998) based on the levels of the compound nucleus ^{10}B with $J^\pi = 1^-, 2^-, 1^+, 2^+, 3^+$, and found that $S(E)$ was mainly dominated by $J^\pi = 1^-$. They deduced $S(0) = 16.9$ and 15.8 MeV·b, respectively, for the ^{9}Be(p, α)^{6}Li and ^{9}Be(p, d)^{8}Be reactions, and gave the screening potential $U_s = 806$ eV. In addition, Xu et al. (2013) also reanalyzed the experimental data (Sierk & Tombrello 1973; Zahnow et al. 1997; Wen et al. 2008) using the distorted-wave Born approximation (DWBA), resulting in $S(0) = 21^{+5}_{-13}$ and 15.4 ± 4 MeV·b for the ^{9}Be(p, α)^{6}Li and ^{9}Be(p, d)^{8}Be reactions, respectively.

Although direct and indirect measurements have been reported in the past, the errors of the $S(E)$ factor are still large at low energies (Sierk & Tombrello 1973; Zahnow et al. 1997; Brune et al. 1998). We recently published results for the ^{9}Be(p, α)^{6}Li reactions from new measurements (Fang et al. 2018). Here we reanalyzed these data, extracted also ^{9}Be(p, d)^{8}Be data and performed a combined R-matrix analysis for both reactions. To improve the precision of reaction rates, more direct measurements of the ^{9}Be(p, d)^{8}Be and ^{9}Be(p, α)^{6}Li reactions are required at as low an energy as possible.

2. Experimental Procedure and Results

The experiment was carried out on the low-energy high-current accelerator at the Research Center for Electron Photon Science of Tohoku University. More details of the accelerator are reported in recent work (Fang et al. 2018) and previously (Yuki et al. 1997; Fang et al. 2011, 2015, 2016; Toriyabe et al. 2012). Figure 1 shows a schematic of the setup in the experimental chamber used in the present work.

Two ion species were used in the experiment. H^+ was used for the proton energy range from 34 to 100 keV amu^{-1}, and H_3^+ from 18 to 34 keV amu^{-1} with 2 keV amu^{-1} increments. The proton beam bends through an angle of 60° with respect to the horizontal plane to bombard the beryllium targets (99%, $0.1 \times 25 \times 25$ mm^3, Nilaco, Tokyo) forming an 8 mm diameter beam-spot. Two silicon surface barrier detectors (300 μm in thickness and 450 mm^2 in area) were installed symmetrically with respect to the beam directions with the detection angle 127°, and with a solid angle ($\Delta\Omega/4\pi$) of about 3%, which was calibrated using the ^{6}Li(d, α)^{4}He reaction at $E_{d\text{-}lab} = 90$ keV occurring in a liquid lithium target. Besides, Al foil of 1 μm thickness was used to prevent the scattered particles from bombarding the detector directly.

The beam current and integrated incident charges were automatically monitored by a Faraday cup every 10 s (Fang et al. 2018). In order to keep the same beam power, the proton beam current was 100 μA at the lowest energies and 18 μA at

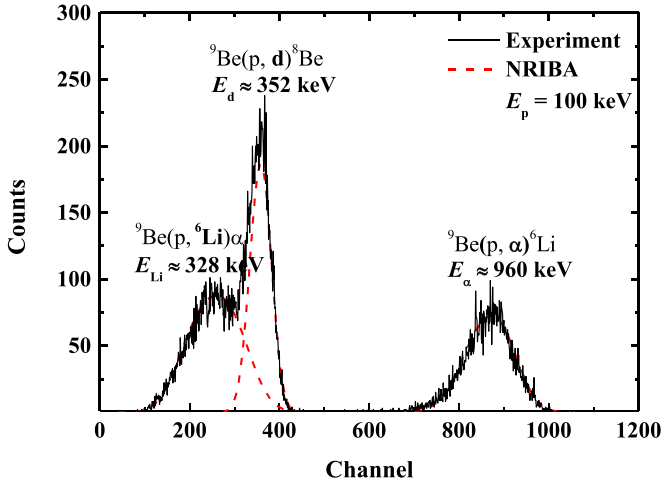

Figure 2. Charged particle spectra obtained at $E_p = 100$ keV. The solid curves represent the experimental results; the dashed curves are the results of the simulation by NRIBA.

highest energies. The stability of the beam current was better than 5% in the bombarding process, but this fluctuation has no influence on the integrated incident charges due to the intervals in the beam current measurements. Meanwhile, the location of the beam-spot for each beam energy was tested and it was found that the spot movement was less than 2 mm. For left–right movement with respect to the horizontal beam direction, the effect on detection efficiency is eliminated using an arrangement of two detectors placed symmetrically relative to the beam direction (inset in Figure 1). For forward–backward movement with respect to the horizontal beam direction, the effect on detection efficiency is estimated to be 3.0% ± 0.2%.

Contamination in the beryllium target, such as injected C and H, significantly affects the screening potential due to the changing of environmental charges. The beryllium target was analyzed before and after irradiation by secondary-ion mass spectrometry. We have found the surface compositions of all the beryllium samples remain almost the same, except for an increase of about 6% in the injected H atoms.

A sample spectrum of the ^{9}Be(p, α)^{6}Li and ^{9}Be(p, d)^{8}Be reactions at $E_p = 100$ keV is shown in Figure 2, which includes three peaks: alpha (α) particles from the ^{9}Be(p, α)^{6}Li reaction, deuterium (d) particles from the ^{9}Be(p, d)^{8}Be reaction, ^{6}Li particles from the ^{9}Be(p, α)^{6}Li reaction as indicated (right to left). However, the peak of the deuteron partly overlaps with ^{6}Li particles because of the resolution of the detector. Therefore, a Monte Carlo spectrum simulation program, Nuclear Reaction Ion Beam Analysis (NRIBA), including the energy loss process, the scattering process, the nuclear reaction process, the detector geometry, and the detector energy resolution, was employed to simulate each peak and analyze the spectrum shown by the dashed curve in Figure 2. More details of NRIBA were reported in our previous work (Wang et al. 2011). In practice, the deuteron counts ($Yield_d(E_i)$) can also be obtained from the overlapped peaks by deducting the lithium ions ($Yield_{Li}(E_i)$) related to the clean alpha-peak ($Yield_\alpha(E_i)$) through the expression for the angular distribution reported by Zahnow et al. (1997). In comparison, the values for $Yield_d(E_i)$ deduced by the above two ways agree with each other within 3% for all the incident energy points. Figure 3 shows the obtained experimental thick-target yields (solid dots).

In general, the values of $S(E_i)$ can be roughly deduced from the thin-target yield $Y_{thin}(E_0)$ through two adjacent thick-target yield points with the assumption that $S(E)$ would be approximately a constant between E and $E + \Delta E$, as follows:

$$Y_{thin}(E_0) = \frac{N_p N_t \Delta\Omega_{lab}}{4\pi} S(E_{eff}) \int_{E_0-\Delta}^{E_0} \frac{d\Omega_{c.m.}}{d\Omega_{lab}} W(\theta, E) \times \frac{1}{E_{c.m.}} \times \exp(-2\pi\eta) \times \left(\frac{dE}{dx}\right)^{-1} dE, \quad (3)$$

where N_p is the number of incident protons, N_t the number density of target atoms, $\Delta\Omega_{lab}$ the solid angle, $d\Omega_{c.m.}/d\Omega_{lab}$ the solid angle ratio of the c.m.-to-lab system, dE/dx the stopping power of Be for a proton, i.e., SRIM code (Ziegler et al. 2008), and $W(\theta, E)$ the angle distribution term reported by Zahnow et al. (1997). E_{eff} is the effective proton energy in this energy interval ($\Delta = 2$ keV) and can expressed as [9]

$$E_{eff} = E_0 - \Delta E + \Delta E \left\{ -\frac{\sigma_2}{\sigma_1 - \sigma_2} + \left[\frac{\sigma_1^2 + \sigma_2^2}{2(\sigma_1 - \sigma_2)^2} \right]^{1/2} \right\}, \quad (4)$$

where σ_1 is the cross section at E_0, and σ_2 corresponds to $E_0 - \Delta E$. Since this energy step is small ($\Delta E = 2$ keV), $S(E_{eff})$ can be considered as constant. Thus, $S(E_{eff})$ can be extracted by fitting the experimental $Yield(E_i)$ using Equation (4). The resulting $S(E_{eff})$ of ^{9}Be(p, α)^{6}Li and ^{9}Be(p, d)^{8}Be reactions are shown as the solid dots (black) in Figure 4, together with the literature data (Sierk & Tombrello 1973; Zahnow et al. 1997; Wen et al. 2008), including direct and indirect measurements. Table 1 summarizes the resulting $S(E_{eff})$ values and compares them with reported values. The errors quoted in the present work arise from statistical uncertainties, detection efficiency and beam current measurement. In addition, all values have a common additional uncertainty of 7.4% due to uncertainties in stopping power (5.4%, mean errors, Ziegler et al. 2008), target deterioration (3%), and angular distribution (4%).

3. Analysis and Discussion

The aim of the present work was to extract the $S(E)$ curves for the reactions ^{9}Be(p, d)^{8}Be and ^{9}Be(p, α)^{6}Li, and a unique screening potential U_s due to the same beryllium environment. Because our data are concentrated in the low-energy region where the screening effect plays a non-negligible role, it is advantageous to combine the present data with the literature $S(E_i)$ measured in the high-energy region, where the screening effect is negligible, to accurately deduce the $S(E)$ over a broad energy region. One can find a reasonable consistency with all data as shown in Figure 4. Furthermore, both our values and reported data were checked by a test of significant differences (F-test), which indicates that our values (18–100 keV) and directly measured high-energy data (100–700 keV) (Sierk & Tombrello 1973; Zahnow et al. 1997) have no significant difference. In the present work, we adopted a full R-matrix to fit all the data (18–700 keV), avoiding the extra uncertainty caused by the extrapolation of bare $S(E)$ in stellar energies.

A multichannel R-matrix code AZURE2 has been used for the R-matrix analysis (Azuma et al. 2010; Uberseder & DeBoer 2015). Resonances in the ^{9}Be(p, α)^{6}Li and ^{9}Be(p, d)^{8}Be reactions adopted in the R-matrix analysis are listed in

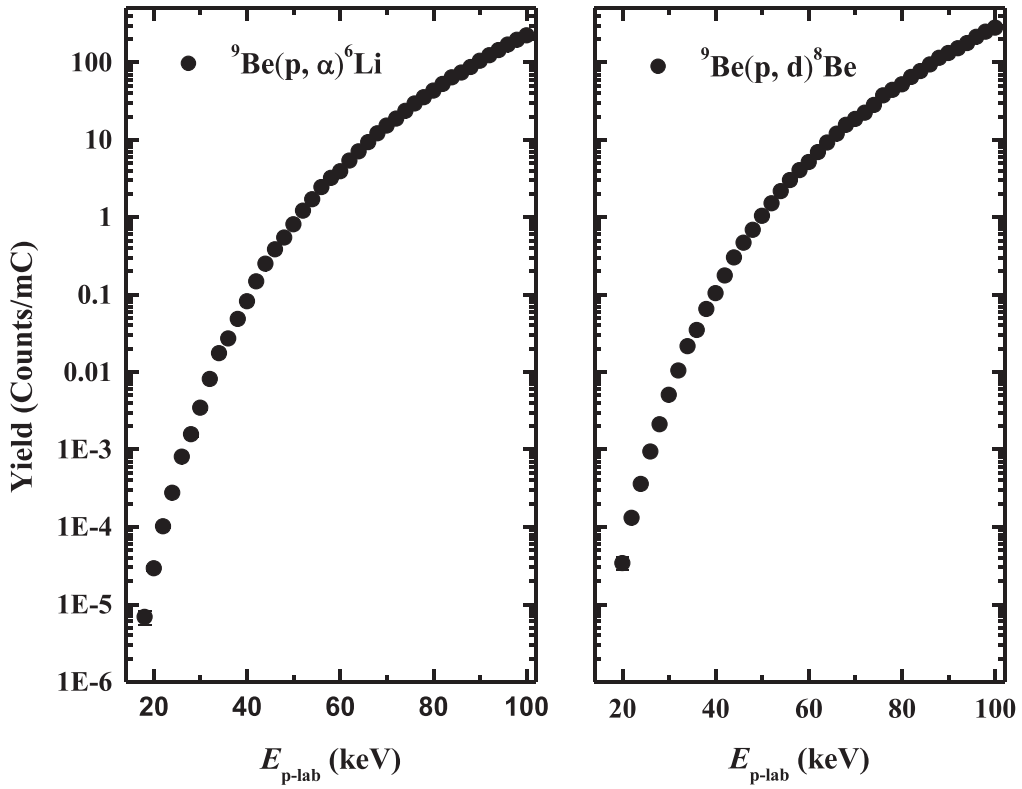

Figure 3. Experimental thick-target yields of the ^{9}Be(p, α)^{6}Li (left) and ^{9}Be(p, d)^{8}Be (right) reactions.

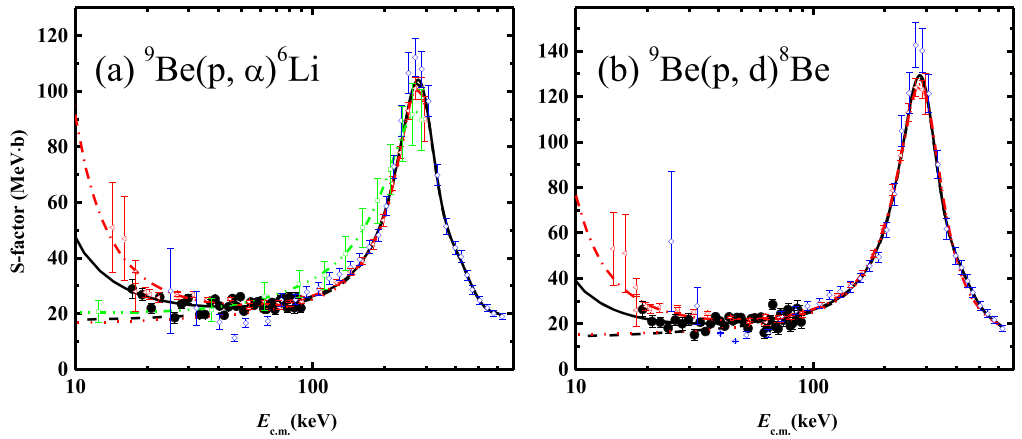

Figure 4. Astrophysical $S(E)$ for the reactions ^{9}Be(p, α)^{6}Li (a) and ^{9}Be(p, d)^{8}Be (b). The solid dots are $S(E_i)$ data deduced experimentally by using Equations (4) and (5) together with the data measured directly (open diamond: Sierk & Tombrello 1973, and open triangle: Zahnow et al. 1997) and indirectly (open square: by THM, Wen et al. 2008). The solid and dashed (black) curves represent $S_{screen}(E)$ and $S_{bare}(E)$ obtained in the present work. The dashed–dotted and dotted (red) curves represent S_{screen} and S_{bare} reported by Zahnow et al. (1997). The dashed–double-dotted curve (green) corresponds to the $S(E)$ factor found by THM (Wen et al. 2008).

Table 2, and the initial input parameters (E_x, J^π, and partial widths) were cited from TUNL Nuclear Data website (Tilley et al. 2004). The values for conventional interaction radius $a_c = 1.45(A_1^{1/3} + A_2^{1/3})$, i.e., $a_p = 4.466$ fm, $a_\alpha = 4.937$ fm, and $a_d = 4.727$ fm, were used. The boundary conditions (B_c values) were chosen equal to the shift factor at an appropriate excitation energy for each J^π value. The excitation energy and partial width were considered as free parameters at $E_x = 6.880$–7.171 MeV, including levels 2^- at 7.171 MeV, 1^- at 6.880 MeV, 1^+ at 6.924 MeV, and 3^+ at 6.992 MeV. All other levels above the fitting energy range were fixed to constrain the R-matrix fit, including the excitation energy and the proton width. It should be noted that the proton width (Γ_p) at $E_x = 8.07$ MeV is not clear ($\Gamma_p/\Gamma = 0.06$–0.2), thus Γ_p was considered as a free parameter. All the partial widths of each level are restricted by the Wigner limit, defined as $\Gamma = 2P_l \times \gamma^2{}_w$, where P_ℓ is the penetrability and $\gamma_w^2 = \frac{3\hbar^2}{2\mu R^2}$.

Finally, an updated spin–parity assignment and width of the resonances at $E_x \approx 6$–9 MeV were obtained from R-matrix fits as shown in Table 2. The obtained excitation energy levels at 6.628 MeV (1^+) and 7.246 MeV (2^-) are different from TUNL Nuclear Data website (6.924 MeV for 1^+, 7.171 MeV for 2^-). The excitation energy of 6.628 MeV (1^+) gives a better description at energies $E_{c.m.} < 300$ keV compared with no such energy level. And the excitation energy 6.628 MeV agrees with Barker's report ($E_r = 6.64$ MeV) where a resonance at $E_p \approx 50$ keV exists. The excitation energy of 7.246 MeV

Table 1
Summary of $S(E)$ for the ^{9}Be(p, α)^{6}Li and ^{9}Be(p, d)^{8}Be Reactions Measured by Direct ($E_{cm} < 700$ keV) and Indirect ($E_{cm} < 1000$ keV) Methods So Far

Direct Measurement												THM	
Present work			69.29	21.46 ± 1.53	18.69 ± 2.40	53.9	24.3 ± 0.6	21.7 ± 0.8	65	17.35 ± 1.73	15.61 ± 1.73	Wen et al.	
E_{cm}	^{9}Be(p, α)^{6}Li	^{9}Be(p, d)^{8}Be	71.09	22.94 ± 1.57	17.83 ± 2.45	62.7	24.3 ± 0.6	23.4 ± 0.8	74	24.90 ± 2.33	23.34 ± 2.33	E_{cm}	^{9}Be(p, α)^{6}Li
17.36	28.89 ± 3.33		72.89	24.88 ± 1.60	24.23 ± 2.50	63.5	22.5 ± 1.3	20.6 ± 1.2	85	24.99 ± 1.79	25.71 ± 1.79	12.5	20.7 ± 4
19.13	26.79 ± 2.16	26.36 ± 3.31	74.69	25.58 ± 1.72	21.60 ± 2.70	71.7	24 ± 0.7	22.6 ± 0.9	94	27.80 ± 1.99	27.80 ± 1.99	37.5	21.3 ± 4
20.90	21.95 ± 1.88	21.03 ± 2.55	78.28	22.04 ± 1.65	26.26 ± 2.75	72.4	22.3 ± 0.8	21.4 ± 0.8	106	28.97 ± 2.23	28.97 ± 2.23	62.5	26.3 ± 5
22.67	25.91 ± 1.74	20.69 ± 2.29	80.08	25.98 ± 1.58	19.06 ± 2.62	80.7	23.3 ± 0.6	22.7 ± 0.9	117	32.69 ± 2.13	32.69 ± 2.13	87.5	30.7 ± 5
26.24	18.58 ± 2.01	21.66 ± 2.48	81.88	24.55 ± 1.69	20.14 ± 2.67	89.6	24.4 ± 0.6	23.4 ± 0.6	130	34.09 ± 2.27	34.09 ± 2.27	112.5	33.8 ± 5
28.02	23.49 ± 1.57	19.98 ± 3.00	83.68	22.14 ± 1.85	22.86 ± 3.05	90	25.6 ± 0.6	25 ± 0.6	144	36.60 ± 2.36	36.31 ± 2.36	137.5	41.6 ± 6
29.81	25.45 ± 1.61	21.95 ± 2.63	85.47	25.71 ± 2.01	26.79 ± 3.28	108	27.8 ± 1.3	28.4 ± 0.9	157	39.49 ± 2.09	40.12 ± 2.09	162.5	51.0 ± 7
33.39	19.58 ± 1.11	20.71 ± 1.56	87.27	23.50 ± 1.85	25.12 ± 2.95	126	31.2 ± 1.2	32.4 ± 1	173	43.99 ± 2.24	45.48 ± 2.24	187.5	60.6 ± 8
35.18	19.69 ± 0.84	16.58 ± 1.25	89.07	22.02 ± 1.46	20.79 ± 2.81	144	35.1 ± 1.3	37.2 ± 1.1	189	48.24 ± 2.19	49.34 ± 2.19	212.5	71.9 ± 9
36.97	24.43 ± 0.71	19.99 ± 1.08				162	39 ± 1.1	42.4 ± 0.9	204	58.74 ± 3.41	61.30 ± 3.41	237.5	84.6 ± 10
38.76	25.26 ± 0.70	23.13 ± 1.05				180	45 ± 1.8	50.6 ± 1.6	219	72.86 ± 4.09	76.94 ± 4.77	262.5	91.7 ± 11
40.56	22.71 ± 0.66	21.21 ± 1.17				198	53.6 ± 2.1	61.6 ± 1.9	236	89.42 ± 5.52	104.88 ± 6.62	287.5	89.7 ± 11
42.35	19.42 ± 0.62	18.97 ± 1.05		Zahnow et al.		216	66.8 ± 2.4	78.7 ± 2.4	253	106.53 ± 7.25	121.49 ± 9.07		
44.14	22.47 ± 0.72	23.00 ± 1.12	14.33	51 ± 16	53 ± 16	234	78 ± 2	94.1 ± 2.1	270	112.18 ± 6.85	142.61 ± 9.89	Romano et al.	
45.94	25.43 ± 0.78	21.33 ± 1.21	16.13	47 ± 15	51 ± 17	252	93 ± 3	113 ± 4	288	107.94 ± 6.44	140.16 ± 9.67	E_{cm}	^{9}Be(p, α)^{6}Li
47.73	22.70 ± 0.83	22.75 ± 1.28	17.92	35 ± 4	36 ± 4	270	101 ± 4	124 ± 4	307	96.48 ± 5.51	121.29 ± 8.27	9.72	13.33 ± 2.76
49.53	26.08 ± 0.73	22.76 ± 1.13	17.93	28 ± 7	26 ± 7	288	101 ± 4	123 ± 4	335	69.79 ± 3.83	90.05 ± 6.08	103	51.65 ± 6.28
51.33	20.87 ± 0.67	20.58 ± 1.05	19.72	27.7 ± 1.7	27.7 ± 1.9	297	90 ± 8	121 ± 9	364	51.40 ± 2.8	61.69 ± 4.67	192	71.42 ± 7.36
54.92	24.16 ± 0.77	22.28 ± 1.21	20.61	26.9 ± 1.9	26.6 ± 2.1				398	43.74 ± 2.34	49.99 ± 3.75	284	68.20 ± 6.9
56.71	23.05 ± 0.71	22.61 ± 1.11	22.4	25.8 ± 1.7	27 ± 2.1				421	40.54 ± 2.10	44.73 ± 3.08	373	56.09 ± 5.98
58.51	24.21 ± 0.72	22.29 ± 1.18	26.87	27.2 ± 0.9	25.9 ± 1.4		Sierk & Tombrello		446	33.87 ± 1.76	38.89 ± 2.76	466	37.55 ± 4.6
60.31	24.53 ± 0.69	22.97 ± 1.12	26.9	26.4 ± 1.2	26.6 ± 1.5	25	28.12 ± 15.3	56.25 ± 30.7	469	28.63 ± 1.6	33.79 ± 2.41	558	28.20 ± 3.68
62.11	21.72 ± 0.74	16.12 ± 2.57	31.37	26.9 ± 1	25.2 ± 1.3	32	21.93 ± 5.98	27.91 ± 7.98	505	24.82 ± 1.42	27.86 ± 2.03	647	20.23 ± 3.37
63.90	21.51 ± 0.75	17.55 ± 2.37	35.84	25.1 ± 0.7	24.6 ± 1.0	40	16.95 ± 2.73	15.86 ± 0.27	542	22.11 ± 1.26	24.37 ± 1.80	736	17.32 ± 3.22
65.70	23.27 ± 0.77	21.82 ± 1.69	44.8	25.3 ± 0.4	22.8 ± 0.6	47	11.30 ± 1.20	12.33 ± 0.12	577	20.10 ± 1.15	21.75 ± 1.64	830	13.18 ± 2.61
67.50	23.99 ± 1.26	28.38 ± 2.15	53.8	22 ± 0.4	20.5 ± 0.5	52	16.66 ± 1.51	15.14 ± 1.51	627	18.97 ± 1.02	17.88 ± 1.46	921	8.43 ± 2.45

Table 2

^{10}B States Reported in the Literature (Tilley et al. 2004) and Obtained from *R*-matrix Fits of the $S(E_i)$ Factor in the Analysis of the ^{9}Be(p, α)^{6}Li and ^{9}Be(p, d)^{8}Be Reactions at E_x = 6–9 MeV Excitation Energy Region

Results from the Literature					Present Work									
J^π	λ	E_λ (MeV)	Γ (keV)	Γ_p/Γ	E_λ (MeV)	Γ_p(keV)		Γ_α (keV)			Γ_d(keV)			Γ (keV)	Γ_p/Γ
						$s = 1$	$s = 2$	$l' = 0$	$l' = 1$	$l' = 2$	$l' = 0$	$l' = 1$	$l' = 2$		
1^-	1	6.880	135	0.27	6.888	33.8			50.0			74.6		158.4	0.21
	2	7.447[a]	130	0.38	7.447[a]	49.4			65.0			1.6		116.0	0.43
2^-	1	7.171	430	≈0.10	7.246		6.5		89.6			43.2		139.3	0.05
	2	7.480[a]	80	0.90	7.480[a]		72		14.4			4.9		91.3	0.79
	3	7.760[a]	245	0.90	7.760[a]		220.5		7.9			0.8		229.2	0.96
1^+	1	6.924	110	≈0.015	6.628			8.4		58.7	183.6		8.6	259.3	≈0[b]
	2	7.66	250	0.3	7.660[a]	44.4	44.5	69.1		4.9	93.7		1.8	258.4	0.34
2^+	1	8.07[a]	1000	0.06–0.2	8.070[a]	84.8	161.5			721.0			123.3	1090.6	0.23
3^+	1	6.992	90	≈0.017	7.009		5.6			99.4			109.9	214.9	0.026

Notes.

[a] These energies are fixed in the fitting process.

[b] The proton width is approximately zero (meV) compared to the total width (keV).

Table 3
$S_{bare}(0)$ and U_s Obtained from the Present Work, Compared with the Values of Earlier Work

The Literature	$S(0)$ (MeV·b)[a]	$S(0)$ (MeV·b)[b]	U_s(eV)
Zahnow et al.	16.1 ± 0.5	14.5 ± 0.5	900 ± 50
Sierk & Tombrello (NACRE)	17^{+25}_{-7}	17^{+25}_{-7}	
Wen et al.	21.0 ± 0.8		676 ± 86
Barker et al.	16.9	15.1	806
NACRE II	21^{+5}_{-13}	15.4 ± 4	
Fang et al.	16.2 ± 1.8, 17.4		545 ± 98
This work	17.3 ± 2.1	13.9 ± 1.8	512 ± 77

Notes.
[a] For ^{9}Be(p, α)^{6}Li.
[b] For ^{9}Be(p, d)^{8}Be.

(2^-) is important for explaining the high-energy tail at $E_p = 360$–700 keV. In addition, the total width of the $J^\pi = 3^+$ state is more than twice as large as the literature reports, which does not significantly affect the $S(E)$ values but can better describe the high-energy data ($E_{c.m.} > 250$ keV). The present results are predominantly interpreted by the 6.888 MeV (1^-) state; other states make smaller contributions to the ^{9}Be(p, α)^{6}Li and ^{9}Be(p, d)^{8}Be reactions.

Figure 4 shows the screened $S_{screen}(E)$ (solid curves) and bare $S_{bare}(E)$ (dashed curves) for both reactions together with the literature results. One may find that: (a) all the direct data are consistent with each other, but not the indirect data (THM); (b) $S_{screen}(E)$ are obviously enhanced in the low-energy region; (c) the enhancement depends on the experimental condition, i.e., $U_s = 512$ eV for ours and $U_s = 900$ eV for Zahnow's.

The resulting $S(E)$ curves agree well with Zahnow et al. (1997) as shown in Figure 4, leading to $S(0) = 17.3 \pm 2.1$ and 13.9 ± 1.8 MeV·b for the Be(p, α)^{6}Li and ^{9}Be(p, d)^{8}Be reactions, respectively. $S(0) = 17.3$ MeV·b is consistent with our previous report (Fang et al. 2018) by resonance-direct analysis (16.2 ± 1.8 MeV b) and R-matrix analysis (17.4 MeV·b) with regard to the ^{9}Be(p, α)^{6}Li reaction. The deduced screening potential $U_s = 512 \pm 77$ eV conforms with our previous report $U_s = 545 \pm 98$ eV within the errors, but is smaller than other reports (900 ± 50 eV for Zahnow's, 806 eV for Barker's, 676 ± 86 eV for Wen's); at the same time all the direct results are larger than the expectation in the adiabatic limit (~264 eV) (Bracci et al. 1990). For comparison, Table 3 summarizes the reported $S_{bare}(0)$ and U_s.

For the long-standing problem of underestimated screening potential, in a simple picture the screened Coulomb potential (ϕ_s) of a Be nucleus can be given by the bare Coulomb potential multiplied by an exponential screened function as $\phi_s = 4e/r \times \exp(-r/\lambda) \approx 4e/r - 4e/\lambda$, where e is the elementary charge, and the screening energy $U_s = 4e/\lambda$ is scaled by the screening length λ, which depends on the surrounding charges (Assenbaum et al. 1987). Thus, all the charges surrounding the target nucleus (Be) would contribute to the screening effect. However, experience shows that the impurity atom (i.e., H) is easily deposited in the solid target, and the target is easily deteriorated/contaminated chemically and changes the surrounding charges. Therefore, both the abnormal screening effect and the large difference between reported values suggest that experimental problems still exist. The most difficult issues in this type of experiment are to determine the density profiles of the target and impurity atoms near the surface of the metal foil, where the reaction mainly occurs. To solve this problem, an inverse kinematic reaction with a beryllium beam bombarding an H_2 target may be useful.

4. Reaction Rate

The abundance of beryllium in the lowest-metallicity stars is a probe of BBN, and also its abundance in halo and disk stars can be significant to the understanding of galactic evolution and stellar structure (Boesgaard & King 1993). Moreover, the surface abundance of ^{9}Be combined with ^{7}Li in stars provides strong constraints on stellar models (the burning temperature of ^{9}Be is $\sim 3.5 \times 10^6$ K, and that of ^{7}Li is $\sim 2 \times 10^6$ K). The surface abundance of ^{9}Be is strongly determined by the adopted physics input, such as the astrophysical reaction rate, the equation of state, the opacity of the stellar matter, as well as external convection efficiencies. The effective energy of astrophysical interest in the p–Be reaction is ~7 keV. However, the reported reaction rate has a large uncertainty (Angulo et al. 1999; Xu et al. 2013) in the astrophysically relevant energy region owing to the extrapolation of the experimental result to low energies.

To facilitate the computation of astrophysics and improve the accuracy of the rates of the ^{9}Be(p, α)^{6}Li and ^{9}Be(p, d)^{8}Be reactions, the reaction rates were calculated using the updated $S(E)$ factor including two parts: the experimental $S(E)$ factor from $E_p = 18$–700 keV and the extrapolated $S(E)$ factor from $E_p = 0$–18 keV obtained from R-matrix fits. The reaction rate $N_A\langle\sigma v\rangle$ was calculated in the temperature range from 0.01 to 1 T_9 by the following formula (Rolfs & Rodney 1988):

$$N_A\langle\sigma v\rangle = \left(\frac{8}{\pi\mu}\right)^{1/2} \frac{N_A}{k_B T_9^{3/2}} \int_0^\infty S_b(E) \times \exp\left(-2\pi - \frac{E}{k_B T_9}\right) dE, \quad (5)$$

where $N_A\langle\sigma v\rangle$ is the reaction rate in unit of cm^3 mol^{-1} s^{-1}, T_9 the temperature in unit of 10^9 K, and $S_b(E)$ the astrophysical factor of the bare nucleus. Figure 5 shows the normalized reaction rate, defined as $N_A\langle\sigma v\rangle_i / N_A\langle\sigma v\rangle_{NACRE}$ and $N_A\langle\sigma v\rangle_i / N_A\langle\sigma v\rangle_{NACREII}$ for both reactions, where $N_A\langle\sigma v\rangle_i$ is deduced in the present work and $N_A\langle\sigma v\rangle_{NACRE}$ is compiled in the standard database (NACRE and NACRE II). The uncertainty consists of two parts: the experimental $S(E)$ uncertainty as shown in Figure 4, and the uncertainty of $S(0)$ obtained from R-matrix fits, which is approximately 13% for ^{9}Be(p, α)^{6}Li and 12% for ^{9}Be(p, d)^{8}Be. The dashed curves represent the uncertainty of the database (NACRE and NACRE II). The present reaction rates of ^{9}Be(p, α)^{6}Li and ^{9}Be(p, d)^{8}Be agree with both compilations given in NACRE and NACRE II (Angulo et al. 1999; Xu et al. 2013). And it is clear that the uncertainty of both reaction rates is significantly reduced, especially for NACRE at temperatures lower than 0.1 T_9. The reason may be the different methods of calculation, e.g., NACRE adopted Sierk's results $S(0) = 17^{+25}_{-7}$ MeV·b for both reactions to calculate the reaction rates at relevant temperatures, while NACRE II excludes Sierk's data at $E_p < 50$ keV, adds THM data ($E_p = 12$–300 keV) (Wen et al. 2008), and adjusts the

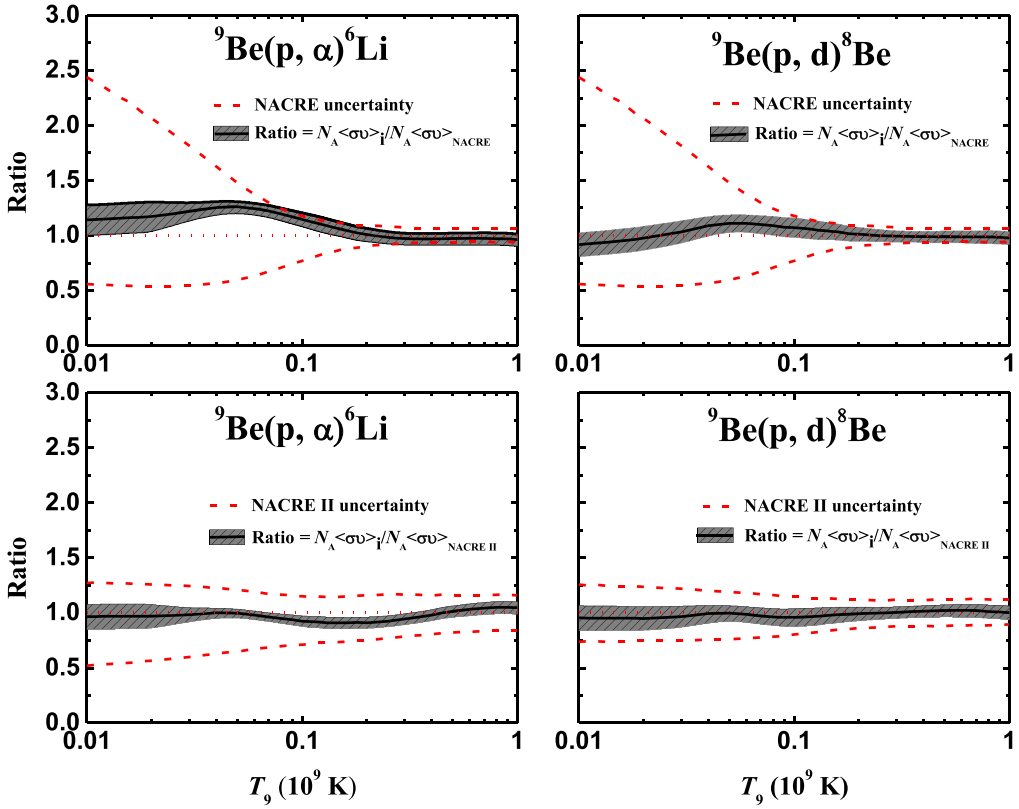

Figure 5. Ratio between the reaction rate extracted by this work and that reported in the standard database (NACRE and NACRE II). The dashed lines represent the uncertainty of NACRE and NACRE II; the shaded areas represent the ratio of the ^{9}Be(p, α)^{6}Li and ^{9}Be(p, d)^{8}Be reaction rates from the present work.

parameters of the DWBA potential model to obtain the reaction rates.

5. Conclusions

The thick-target yields of the ^{9}Be(p, α)^{6}Li and ^{9}Be(p, d)^{8}Be reactions were measured in the energy range 18–100 keV. Further, we obtained the astrophysical $S(E_{\rm eff})$ factor of these two reactions from the thin-target yield, which is consistent with direct measurement. Combining the present result with high-energy data, we performed a full R-matrix analysis in the proton energy range $E_{\rm p} < 700$ keV for the ^{9}Be(p, α)^{6}Li and ^{9}Be(p, d)^{8}Be reactions to improve the resonance parameters of the excited state at $E_{\rm x} \approx 6$–9 MeV of ^{10}B. The present results are predominantly interpreted by the 6.888 MeV (1^-) state. The extracted $S(E)$ factors of the ^{9}Be(p, α)^{6}Li and ^{9}Be(p, d)^{8}Be reactions, resulting in $S(0) = 17.3 \pm 2.1$ and 13.9 ± 1.8 MeV·b, respectively, agree with direct measurement. The resulting $U_{\rm s} = 512 \pm 77$ eV is much larger than the expectation in the adiabatic limit (∼264 eV) and different from other reports (Zahnow's 900 ± 50 eV, Barker's 806 eV, and Wen's 676 ± 86 eV), owing to the different experimental conditions. In addition, the rates of the ^{9}Be(p, α)^{6}Li and ^{9}Be(p, d)^{8}Be reactions have been updated and the present results improve the accuracy compared with the standard database (NACRE and NACRE II).

This work was supported by the Major State Basic Research Development Program of China (2016YFA0400503), the Fundamental Research Funds for the Central Universities (lzujbky-2019-53), the National Natural Science Foundation of China under grants No. 11705244 and the Youth Innovation Promotion Association of Chinese Academy of Sciences under grant No. 2019406. It has also been supported by the Science Challenge Project (no. TZ2018005).

ORCID iDs

Qian Zhang https://orcid.org/0000-0002-3754-3557

References

Angulo, C., Arnould, M., Rayet, M., et al. 1999, NuPhA, 656, 3
Assenbaum, H. J., Langanke, K., & Rolfs, C. 1987, ZPhyA, 327, 461
Azuma, R. E., Uberseder, E., Simpson, E. C., et al. 2010, PhRvC, 81, 045805
Barker, F. C., & Kondō, Y. 2001, NuPhA, 688, 959
Baur, G. 1986, PhLB, 178, 135
Boesgaard, A. M., & King, J. R. 1993, ApJ, 106, 2309
Boyd, R. N., & Kajino, T. 1989, ApJL, 336, L55
Bracci, L., Fiorentini, G., Melezhik, V. S., et al. 1990, NuPhA, 513, 316
Brown, E. F. 1998, ApJ, 495, 905
Brune, C. R., Geist, W. H., Karwowski, H. J., et al. 1998, PhRvC, 57, 3437
Causey, R. A. 2002, JNuM, 300, 91
Coc, A., Goriely, S., Xu, Y., et al. 2012, ApJ, 744, 158
Copi, C. J., Schramm, D. N., & Turner, M. S. 1995, Sci, 267, 192
Fang, K., Wang, T., Yonemura, H., et al. 2011, JPSJ, 80, 084201
Fang, K., Zhang, Q., Chen, B., et al. 2018, PhLB, 785, 262
Fang, K., Zou, J., He, H., et al. 2016, PhRvC, 94, 054602
Fang, K., Zou, J., Liu, D., et al. 2015a, ChPhC, 39, 084001
Fang, K., Zou, J., Yoshida, E., et al. 2015b, EL, 109, 22002
Federici, G., Skinner, C. H., Brooks, J. N., et al. 2001, NuFu, 41, 1967
Fowler, W. A. 1984, RMPh, 23, 645
Ichimaru, S. 2008, RvMP, 54, 1017
Kajino, T., & Boyd, R. N. 1990, ApJ, 359, 267
Kasagi, J. 2004, PThPS, 154, 365
Kittel, C. 1986, Introduction to Solid State Physics (6th ed.; New York: Wiley)
Lamia, L., Spitaleri, C., Tognelli, E., et al. 2015, ApJ, 811, 99
Pizzone, R. G., Spitaleri, C., Lattuada, M., et al. 2004, A&A, 398, 423

Primas, F., Duncan, D. K., Pinsonneault, M. H., et al. 1997, ApJ, 480, 784
Raiola, F., Gang, L., Bonomo, C., et al. 2004, EPJA, 19, 283
Rauscher, T., Applegate, J. H., Cowan, J. F., et al. 1994, ApJ, 429, 499
Rolfs, C. E., & Rodney, W. S. 1988, Theoretical Astrophysics (Chicago, IL: Univ. Chicago Press), 42
Romano, S., Lamia, L., Spitaleri, C., et al. 2006, EPJA, 27, 221
Salpeter, E. E. 1954, AuJPh, 7, 373
Sierk, A. J., & Tombrello, T. A. 1973, NuPhA, 210, 341
Spitaleri, C., Mukhamedzhanov, A. M., Blokhintsev, L. D., et al. 2011, PAN, 74, 1725
Stephens, A., Boesgaard, A. M., King, J. R., & Deliyannis, C. P. 1997, ApJ, 491, 339
Thomas, D., Schramm, D. N., Olive, K. A., et al. 1994, ApJ, 430, 291
Tilley, D. R., Kelley, J. H., Godwin, J. L., et al. 2004, NuPhA, 745, 155
Toriyabe, Y., Yoshida, E., Kasagi, J., et al. 2012, PhRvC, 85, 054620
Uberseder, E., & DeBoer, R. J. 2015, AZURE User Manual, https://azure.nd.edu/login.php
Wang, T. S., Guan, X. C., Fang, K. H., et al. 2012, JPhG, 39, 015201
Wang, T. S., Zhao, J. T., Lan, M. C., et al. 2011, NIMPB, 269, 2721
Wen, Q. G., Li, C. B., Zhou, S. H., et al. 2008, PhRvC, 78, 035805
Wu, Y. 2007, FE&D, 82, 1893
Xu, Y., Takahashi, K., Goriely, S., et al. 2013, NuPhA, 918, 61
Yuki, H., Sato, T., Ohtsuki, T., et al. 1997, JPSJ, 66, 73
Zahnow, D., Rolfs, C., Schmidt, S., et al. 1997, ZPhyA, 359, 211
Ziegler, J. F., Ziegler, M. D., & Biersack, J. P. 2008, SRIM - The Stopping and Range of Ions in Matter, 268 (Chester, MD: SRIM Co.)